Characterization in Non-human Primates of (R)-[18F]OF-Me-NB1 and (S)-[18F]OF-Me-NB1 for Imaging the GluN2B Subunits of the NMDA Receptor

Ming-Qiang Zheng
Yale University School of Medicine https://orcid.org/0000-0002-2814-8213
Hazem Ahmed
Institution of Pharmaceutical Sciences, ETH Zurich
Kelly Smart
Yale University School of Medicine
Yuping Xu
Jiangsu Institute of Nuclear Medicine
Daniel Holden
Yale University School of Medicine
Michael Kapinos
Yale University School of Medicine
Zachary Felchner
Yale University School of Medicine
Ahmed Haider
Institute of Pharmaceutical Sciences,ETH Zurich
Gilles Tamagnan
Yale University School of Medicine
Richard E. Carson
Yale University School of Medicine
Yiyun Huang
Yale University School of Medicine
Simon M. Ametamey (simon.ametamey@pharma.ethz.ch)
Institution of Pharmaceutical Sciences,ETH Zurich https://orcid.org/0000-0003-4285-6731

Research Article

Keywords: [18F]OF-Me-NB1, GluN2B Subunit, NMDA Receptor, PET imaging, non-human primates

Posted Date: November 17th, 2021

DOI: https://doi.org/10.21203/rs.3.rs-1068936/v1

Abstract

Purpose

GluN2B containing *N*-methyl-*D*-aspartate receptors (NMDARs) play an essential role in neurotransmission and are a potential treatment target for multiple neurological and neurodegenerative diseases, including stroke, Alzheimer's disease, and Parkinson's disease. In a previous report (*R*)-[^{18}F]OF-Me-NB1 was reported to be more specific and selective for targeting the GluN2B subunits of the NMDAR. Here we report a comprehensive evaluation of (*R*)-[^{18}F]OF-Me-NB1 and (*S*)-[^{18}F]OF-Me-NB1 in non-human primates.

Methods

The radiosynthesis of (*R*)-[^{18}F]OF-Me-NB1 and (*S*)-[^{18}F]OF-Me-NB1 was accomplished as reported previously with minor modifications. PET scans in two rhesus monkeys were conducted on the Focus 220 scanner. Blocking studies were performed after treatment of the animals with the GluN2B antagonist Co101,244 or the sigma-1 receptor antagonist FTC-146. One-tissue (1T) compartment model and multilinear analysis-1 (MA1) method with arterial input function were used to obtain regional volume of distribution (V_T, mL/cm^3). Occupancy values by the two blockers were obtained by the Lassen plot. Regional non-displaceable binding potential (BP_{ND}) was calculated from the corresponding baseline V_T and the V_{ND} derived from the occupancy plot of the Co101,244 blocking scans.

Results

(*R*)- and (*S*)-[^{18}F]OF-Me-NB1 were produced in >99% radiochemical and enantiomeric purity, with molar activity of 224.22 ± 161.69 MBq/nmol at the end of synthesis (n=10). Metabolism was moderate, with ~30% parent compound remaining for (*R*)-[^{18}F]OF-Me-NB1 and 20% for (*S*)-[^{18}F]OF-Me-NB1 at 30 min post injection. Plasma free fraction was 1-2%. In brain regions both (*R*)- and (*S*)-[^{18}F]OF-Me-NB1 displayed fast uptake with slower clearance for the (*R*)- than (*S*)-enantiomer. For (*R*)-[^{18}F]OF-Me-NB1, both the 1T model and MA1 method gave reliable estimates of regional V_T values, with MA1 V_T (mL/cm^3) ranging from 8.9 in the cerebellum to 12.8 in the cingulate cortex. Blocking with 0.25 mg/kg of Co101,244 greatly reduced the uptake of (*R*)-[^{18}F]OF-Me-NB1 across all brain regions, resulting in an occupancy of 77% and V_{ND} of 6.36, while 0.027 mg/kg of FTC-146 reduced specific binding by 30%. Regional BP_{ND}, as a measure of specific binding signals, ranged from 0.40 in the cerebellum to 1.01 in the cingulate cortex.

Conclusions

In rhesus monkeys, (*R*)-[^{18}F]OF-Me-NB1 exhibited fast kinetics and heterogeneous uptake across brain regions, while the (S)-enantiomer displayed a narrower dynamic range of uptake across regions. Blocking study with a GluN2B antagonist indicated binding specificity. Value of BP_{ND} were >0.5 in most brain regions, suggesting good *in vivo* specific binding signals. Taken together, results from the current study

demonstrated the potential of (*R*)-[^{18}F]OF-Me-NB1 as a useful radiotracer for imaging the GluN2B receptor.

Introduction

There have been great research efforts to develop suitable Positron Emission Tomography (PET) imaging agents targeting the *N*-methyl-*D*-aspartate receptor (NMDAR) complex. Radioligands developed to date have targeted mainly the 1) PCP-binding site, 2) glutamate-binding site, 3) glycine-binding site and 4) ifenprodil-binding site [1-6]. Ligands developed for the ifenprodil-binding site are specific to the GluN2B subunits of NMDAR. This receptor subtype is a potential treatment target for multiple neurological and neurodegenerative diseases, including stroke, Alzheimer's disease (AD), and Parkinson's disease (PD) [7-12]. In the adult brain the GluN2B subunit is mainly expressed in the forebrain, a region that regulates cognitive functions. Therefore, GluN2B selective antagonists have been developed as potential therapeutic agents for the treatment of cognitive deficits with an improved safety profile [13]. Active research has also been directed at the development of PET imaging agents to assist in the screening and optimization of drug candidates. However, despite more than 20 years of intensive efforts, no suitable GluN2B PET imaging agents are available for clinical research. The primary reasons for the failures are: 1) Low brain uptake of the radioligands. 2) brain uptake pattern inconsistent with known GluN2B expression; 3) off-target binding *in vivo*, especially to sigma-1 receptor; 4) presence of radioactive metabolite(s) in the brain [14-16].

Ifenprodil is an inhibitor of the GluN2B subunit-containing NMDARs (K_i: 10 nM) [11]. Modifications of ifenprodil resulted in compounds with preferred binding to either GluN2B subunit or sigma-1 receptor [17-19]. Our group previously reported [^{11}C]Me-NB1, a racemic GluN2B antagonist derived from ifenprodil, with high binding affinity to GluN2B (K_i: 5.4 nM) and selectivity over sigma-1 and sigma-2 receptors (K_i: 182 and 554 nM, respectively) [20]. The (*R*)-enantiomer of [^{11}C]Me-NB1 was demonstrated in rodents to have good brain uptake and higher specific binding signals than the (*S*)-enantiomer, and has recently been evaluated in humans[21]. Further structural modifications of [^{11}C]Me-NB1 led to compounds suitable for labeling with the longer half-life ^{18}F-nuclide, and thus the discovery of [^{18}F]OF-Me-NB1 [Fig. 1] [22]. Similar to [^{11}C]Me-NB1, the (*R*)-enantiomer of [^{18}F]OF-Me-NB1 was found to have high binding affinity to GluN2B (K_i: 4 nM) and high selectivity over sigma-1 receptor (K_i: 100 nM). Both *in vitro* and *in vivo* studies in rodents indicated (*R*)-[^{18}F]OF-Me-NB1 as a promising radiofluorinated PET tracer for imaging the GluN2B subunit-containing NMDARs. In the current study, we investigated (*S*)-[^{18}F]OF-Me-NB1 and (*R*)-[^{18}F]OF-Me-NB1 in non-human primates.

Materials And Methods

Chemistry

Synthesis of the racemic and enantiopure (*R*)- and (*S*)-OF-Me-NB1, and their corresponding aryl boronic esters as precursors followed the previously reported procedure[23]. The absolute configuration of (-)-OF-Me-NB1 and (+)-OF-Me-NB1 were confirmed by circular dichroism.

Radiochemistry

$H_2{}^{18}O$ was obtained from Huayi Isotopes (Toronto, Canada). Anion exchange Chromafix cartridges (PS-HCO_3) were purchased from Macherey-Nagel (Dueringen, Germany). Solid-phase extraction (SPE) cartridges were purchased from Waters Corporation (Milford, MA, USA). The HPLC system used for purification of the tracers included a Shimadzu LC-20A pump, a Knauer K200 UV detector, and a Bioscan g-flow detector, with a semi-preparative HPLC column (Agilent XDB, 9.4 x 250 mm, 5 mm; mobile phase: 27/73 acetonitrile/0.1M ammonium formate with 5% acetic acid, pH 4.2; flow rate; 5 mL/min). The HPLC system used for quality control analysis includes a Shimadzu LC-20A pump, a Shimadzu SPD-M20A PDA or SPD-20AUV detector (wavelength set at 230 nm), a Bioscan g-flow detector, with a Luna C18(2) column (5 mm, 4.6 x 250 mm) eluting with 36/64 acetonitrile/0.1M ammonium formate with 5% acetic acid, pH 4.2, at a flow rate of 2 mL/min. The chiral purity was determined by chiral HPLC with a Regis Pack column (5 mm, 4.6 x 250 mm) eluting with 85/15 hexane/ethanol at a flow rate of 1 mL/min.

[^{18}F]Fluoride was produced via the $^{18}O(p,n)^{18}F$ nuclear reaction in a 16.5 MeV GE PETtrace cyclotron (Uppsala, Sweden). The cyclotron produced aqueous [^{18}F]fluoride solution in [^{18}O]water was trapped on the anionic exchange resin cartridge, then eluted off with a solution of Kryptofix 222 (6.3 mg/mL in acetonitrile), $K_2C_2O_4$ (1.0 mg/mL in water), and K_2CO_3 (0.1 mg/mL in water) to a 5 mL borosilicate glass reaction vial. The elution solution was evaporated at 110 ^{o}C for about 5 min under a nitrogen stream, followed by azeotropic drying with two sequential additions of 0.4 mL acetonitrile. After cooling, 20 mL of air was pushed to the reaction vial, followed by a solution of the boronic ester precursor (6 mg) and $Cu(OTf)_2(Py)_4$ (12 mg) in of anhydrous dimethylacetamide (0.4 mL). The mixture was stirred and heated at 120 ^{o}C for 20 min and quenched with acetonitrile/water (1:1, v/v, 0.8 mL). A solution of 10 N NaOH (0.4 mL) was added to the reaction vial and the mixture stirred at 90 ^{o}C for 15 min. After neutralization with 8 N HCl (0.5 mL), the crude reaction mixture was purified by semi-preparative HPLC. The radioactive product peak from 24-29 min was collected and diluted with 50 mL of water. The solution was passed through a Waters C18 SepPak cartridge. The SepPak was washed with 1 mM HCl (10 mL) and dried with air. The product was eluted off the SepPak with 1 mL of USP EtOH, followed by 3 mL of USP saline. The combined solution was then passed through a 0.22 mm GV filter (Millipore, Sigma) into a 10 mL dose vial pre-charged with 7 mL of USP saline. For determination of enantiomeric purity, an aliquot of the EtOH solution was diluted with hexane/ethanol (85/15, v/v) and analyzed by chiral HPLC.

Measurement of Lipophilicity (log $D_{7.4}$)

Lipophilicity (log $D_{7.4}$) was measured using the flash-shake method according to the procedure previously reported[24]. Log $D_{7.4}$ was calculated as the ratio of decay-corrected radioactivity concentrations in 1-

octanol and phosphate buffered saline (PBS, pH = 7.4, Dulbecco). Six consecutive equilibrations were performed until a constant value of log $D_{7.4}$ was obtained.

PET Imaging in Rhesus Monkeys

A total of seven PET scans in two monkeys were acquired. Each monkey underwent one baseline scan with (*R*)-[^{18}F]OF-Me-NB1, and two blocking scans at 10 min after the injection of the GluN2B antagonist Co-101,244 (0.25 mg/kg) or the sigma1R antagonist FTC-146 (0.027 and 0.125 mg/kg). In addition, a baseline scan with (*S*)-[^{18}F]OF-Me-NB1 was also performed in one monkey. All procedures were approved by the Yale University Institutional Animal Care and Use Committee.

Animals were sedated with a combination of alfaxalone (2 mg/kg), midazolam (0.3 mg/kg) and dexmedetomidine (0.01 mg/kg) and maintained in an anesthetized state with 1.5-2.5% isoflurane in oxygen. Heart rate, blood pressure, respiration rate, oxygen saturation and respiration rate were monitored continuously. An arterial line was placed in the radial artery for blood sampling.

Dynamic PET data were acquired on the Focus 220 scanner (Siemens Medical Solutions, Knoxville, TN, USA). Before radiotracer injection, a 9 min transmission scan was obtained for attenuation correction. The radiotracer (10 mL) was administered intravenously as a slow bolus over 3 min. Emission data were collected in list mode for 90 or 120 min and binned into frames of increasing durations (6 × 30 s, 3 × 1 min, 2 × 2 min, 22 × 5 min).

Arterial Input Function Measurement and Metabolite Analysis. Measurements of plasma activity and parent fraction over time were performed as previously described [25, 26]. Arterial or venous blood samples were collected at preselected time points and assayed for radioactivity in whole blood and plasma with cross-calibrated gamma counters (Wizard 1480/2480, Perkin Elmer, Waltham, MA, USA). The volume of the whole blood or plasma (50-200 µL) was determined by the weight of the sample. Parent fraction was calculated as the ratio of the total radioactivity in fractions containing the parent compound to the total amount of radioactivity collected and fitted with an inverted gamma function and corrected for filtration efficiency. The arterial plasma input function (AIF) was then calculated as the product of the total counts in the plasma and the interpolated parent fraction at each time point.

Measurement of Radiotracer Free Fraction (f_p) in Plasma. Ultrafiltration method was used for measuring the unbound portion (free fraction) of [^{18}F]OF-Me-NB1 in plasma as previously described [24]. The f_P was determined as the ratio of the radioactivity concentration in the filtrate to the total activity in plasma. Measurements of f_P were performed in triplicate for each scan.

Image processing. High resolution magnetic resonance images were acquired with a Siemens 3T Trio scanner for region of interest (ROI) definition. PET emission data were attenuation-corrected using the transmission scan, then reconstructed using a Fourier rebinning and filtered back-projection algorithm. PET images summed from the first 10 minutes of each scan were registered to the anatomical MR image. Inverted transformations were applied to register an atlas ROI mask to the PET image, and time-activity

curves (TACs) were extracted from each ROI: frontal, occipital, temporal, cingulate, and insular cortex, caudate, putamen, globus pallidus, nucleus accumbens, amygdala, hippocampus, thalamus, pons, substantia nigra, cerebellum, and centrum semiovale.

Kinetic modeling. Kinetic parameters were determined by fitting the regional TACs and metabolite-corrected arterial input functions to the one-tissue compartment (1TC) and two-tissue compartment (2TC) models, as well as the multilinear analysis 1 (MA1) method with starting time of 30 min [27]. Regional volume of distribution (V_T, mL/cm^3) was derived in each case.

For the blocking studies, occupancy plots were constructed using regional V_T values at baseline and difference in V_T between baseline and blocking scans. Percent target occupancy across the brain and non-displaceable volume of distribution (V_{ND}) were then determined from the resulting linear relationship [28].

Results

Chemistry

Enantiomeric pure (*R*)- and (*S*)-OF-Me-NB1 and their boronic ester radiolabeling precursors were prepared in good chemical yields as previously reported [14].

Radiochemistry

Both (*R*)- and (*S*)-[^{18}F]OF-Me-NB1 were prepared in 11 ± 3.5% radiochemical yield (n=10, decay-uncorrected). Radiochemical purity was greater than 99%, with molar activity of 224.22 ± 161.69 MBq/nmol at the end of the synthesis (EOS, *n* = 10). Total synthesis time was about 100 min including purification and product formulation. There was no racemization during the radiolabeling and deprotection step. Enantiomeric purity was > 98% for both (*R*)- and (*S*)-[^{18}F]OF-Me-NB1, as determined by chiral HPLC analysis (Fig. 2).

Measurement of log $D_{7.4}$

The measured log $D_{7.4}$ value was 2.85 ± 0.01 (n = 4) for (*R*)-[^{18}F]OF-Me-NB1. This value is within the range of brain-penetrating radioligands.

PET Imaging Experiments in Rhesus Monkeys

Injection Parameters. The injected activity ranged from 122 MBq to 174 MBq, corresponding to injection mass of 0.01-0.05 ug/kg.

Plasma Analysis. Figure 3 shows the parent fraction of (*R*)- and (*S*)-[^{18}F]OF-Me-NB1 over time in the same monkey. At 30 min after tracer injection, parent (*R*)-[^{18}F]OF-Me-NB1 represented about 30% of the total plasma activity in the baseline scans, which further decreased to 20% at 90 min. Parent fraction of (*S*)-

[^{18}F]OF-Me-NB1 was lower than the (*R*)-enantiomer, at ~20% at 30 min and ~10% at 90 min post injection. Pretreatment with the NMDA GluN2B blocking drug Co101,244 appeared to accelerate the decrease in parent fraction. On the other hand, pretreatment with FTC-146 had little effect. Plasma free fraction was 1.2 ± 0.2% (n= 6) for (*R*)-[^{18}F]OF-Me-NB1 and 1.8% (n= 1) for (*S*)-[^{18}F]OF-Me-NB1.

Brain Analysis. In the monkey brain, (*R*)-[^{18}F]OF-Me-NB1 displayed good uptake and a heterogeneous distribution pattern (Fig. 4, top right). (*S*)-[^{18}F]OF-Me-NB1 also displayed good brain uptake and a more homogenous distribution pattern, consistent with the results from rodents (Fig. 4, bottom left).

The regional time-activity curves (TACs) from the baseline scans of (*R*)- and (*S*)-[^{18}F]OF-Me-NB1 are also shown in Figure 4. (*R*)-[^{18}F]OF-Me-NB1 displayed fast and high brain uptake, as well as fast clearance. Peak uptake SUV of 4.5-6.5 across brain regions was reached within 20 min after tracer injection. Higher activity concentrations were found in the cingulate cortex, medium in the frontal cortex, hippocampus, and putamen, and low in the cerebellum, which is consistent with the expression of GluN2B subunits in the brain. (*S*)-[^{18}F]OF-Me-NB1 also displayed fast and high brain uptake, and fast clearance, with peak SUV of 3.0-4.5 across regions reached within 15 min. In comparison with (*R*)-[^{18}F]OF-Me-NB1, the dynamic range of (*S*)-[^{18}F]OF-Me-NB1 uptake across regions was narrower, indicating lower levels of specific binding. Therefore, subsequent experiments were performed with (*R*)-[^{18}F]OF-Me-NB1 only.

The blocking studies were conducted using the GluN2B antagonist Co101,244 and the selective sigma-1 receptor antagonist FTC-146 [29, 30]. Pretreatment with Co101,244 (0.25 mg/kg) reduced the uptake of (*R*)-[^{18}F]OF-Me-NB1 in all brain regions to nearly homogenous levels (Fig. 5, middle). Interestingly, FTC-146 also appeared to reduce the uptake of (*R*)-[^{18}F]OF-Me-NB1 in all brain regions, although by a smaller magnitude compared to Co101,244 (Fig. 5, right). These trends were seen more clearly on the TACs. Co101,244 reduced activity concentrations in high and medium uptake brain regions to the same levels as those in the cerebellum and semiovale (white matter region) at the end of the scan, while FTC-146 induced partial reduction in radioactivity uptake across brain regions.

Time-activity curves were analyzed with 1TC, 2TC and MA1 method to generate binding parameters using the metabolite-corrected plasma activity as input function. The 1TC and MA1 model showed better fits of the TACs than the 2TC model and values showed good agreement between the two. Thus the MA1 was chosen as a suitable and reliable model for quantitative analysis. Regional V_T values derived from MA1 analysis (t^* = 30 min) are listed in Table 1. In the baseline scans, regional V_T values followed the order of cingulate cortex > putamen > hippocampus > frontal cortex > thalamus > semiovale > cerebellum, which is consistent with the regional expression of GluN2B subunits in the brain [16]. Blocking with either Co101,244 or FTC-146 led to decreased V_T values across all brain regions, with Co101,244 producing more pronounced decrease than FTC-146.

Receptor occupancy by different blocking drugs was calculated using the occupancy plot (Fig. 6). In the male monkey (monkey 1), 0.25 mg/kg of Co101,244 resulted in 77% occupancy with V_{ND} of 6.4 mL/cm^3,

while a low dose of FTC-146 (0.027 mg/kg) gave about 30% occupancy. In the female monkey (monkey 2), Co101,244 at the same 0.25 mg/kg dose produced an occupancy of 68%, with the same V_{ND} of 6.4 mL/cm^3. In this animal, a higher dose of FTC-146 (0.125 mg/kg) gave similar level of occupancy, 33%, to the low dose in the male monkey. This indicates that the sigma-1 receptor antagonist does not produce a dose-response occupancy pattern for the (*R*)-[^{18}F]OF-Me-NB1 in the monkey brain.

Regional values of non-displaceable binding potential (BP_{ND}) were calculated using the V_{ND} values derived from the occupancy plots (Table 1). The rank order of regional BP_{ND} values was the same as that for V_T, and consistent in both the male and female monkeys. These data demonstrate that in the monkey brain, (*R*)-[^{18}F]OF-Me-NB1 specifically and selectively binds to GluN2B receptor, and the specific binding can be reliably measured in monkey brain regions.

Table 1 MA1-derived distribution volume (V_T) and non-displaceable binding potential (BP_{ND}) of (*R*)-[^{18}F]OF-Me-NB1 across brain regions in two rhesus monkeys

	V_T (mL/cm^3) and BP_{ND} monkey1/monkey2			
Region of Interest (ROI)	Baseline	Co101,244	FTC-146	BP_{ND}
Cerebellum	8.9/9.2	6.9/7.6	9.3/8.7	0.40/0.43
Cingulate cortex	12.8/12.2	8.1/7.9	11.6/10.1	1.01/0.90
Frontal cortex	10.7/10.3	6.8/7.4	9.4/9.2	0.68/0.60
Hippocampus	11.0/10.3	6.9/7.3	10.5/9.2	0.73/0.60
Putamen	11.2/10.3	8.1/8.2	11.0/9.5	0.76/0.60
Semiovale	9.1/9.5	8.6/8.0	9.5/8.4	0.43/0.48
Thalamus	9.4/9.6	6.8/6.8	9.4/8.6	0.48/0.50

Discussion

The GluN2B subunits of the NMDAR play an important role in neurodegenerative diseases, thus the development of diagnostic and therapeutic agents targeting this receptor will be valuable for the elucidation of its involvement in diseases. OF-Me-NB1, a close analog of Me-NB1, showed promising *in vitro* binding specificity to GluN2B subunits and selectivity over sigma1 receptor. The binding affinity (K_i, nM) of (*R*)-OF-Me-NB1 for GluN2B was 4 nM and 37 nM for (*Rac*)-OF-Me-NB1. The K_i for (*S*)-OF-Me-NB1 is not measured but expected to be one-fold lower than the *R* enantiomer, based on the affinity value of the racemic mixture. The selectivity over sigma-1 receptor of (*R*)-OF-Me-NB1 was >100 nM (32 nM for (*Rac*)-OF-Me-NB1) [22]. (*R*)- and (*S*)-OF-Me-NB1 were previously labeled with either carbon-11 or fluorine-18 and evaluated in rodents. Carbon-11 or fluorine-18 labeled OF-Me-NB1 exhibited distinct binding patterns consistent with GluN2B distribution and selectivity over sigma-1 receptors on rodent brain tissues, while

(*S*)-[^{11}C]OF-Me-NB1 showed a more homogenous distribution and binding to sigma-1 receptor. The excellent binding properties of (*R*)-[^{18}F]OF-Me-NB1 observed in rodent brain prompted us to fully evaluate this tracer in non-human primates with the aim to possibly advance it to human studies.

Although (*S*)-[^{11}C]OF-Me-NB1 did not show promising attributes in rodents, we nonetheless decided to evaluate the fluorine-18 labeled version given that the position of label potentially could make a difference in the performance characteristics of (*S*)-[^{18}F]OF-Me-NB1 in the non-human primate brain. As such, both (*S*)- and (*R*)-[^{18}F]OF-Me-NB1 were prepared using enantiopure acetyl protected boron pinacol ester precursors in a two-step, one-pot radiosynthetic approach. Both radioligands were obtained in >99% radiochemical and enantiomeric purities, with molar activity of 224.22 ± 161.69 MBq/nmol. PET imaging studies in rhesus monkeys demonstrated that (*S*)-[^{18}F]OF-Me-NB1 appeared to have less specific binding in the monkey brain, consistent with the results from previously reported rodent study. In comparison, (*R*)-[^{18}F]OF-Me-NB1 displayed higher specific binding that could be blocked by a GluN2B antagonist. The rapid brain uptake and clearance of (*R*)-[^{18}F]OF-Me-NB1 in major brain regions indicates proper *in vivo* kinetics for future study in measuring small receptor changes. (*R*)-[^{18}F]OF-Me-NB1 exhibited a favorable metabolic profile and acceptable plasma free fraction. All the radioactive metabolites were more polar than the parent tracer, thus less likely cross the blood-brain barrier in the monkey brain. 1T and MA1 analysis gave reliable and comparable V_T for both the male and the female monkey. High V_T values were found in the forebrain, including cingulate cortex, putamen and frontal cortex, and medium to low in white matter (semiovales) and cerebellum. The value of regional BP_{ND}, as a measure of specific binding signals, ranged from 1.0 in cingulate cortex to 0.4 in cerebellum in the male monkey, and 0.90 in cingulate cortex to 0.43 in cerebellum in the female monkey. This result indicates similar specific binding signals between sexes in non-human primates. The pattern of the specific binding at different brain regions is consistent to the pattern of GluN2B expression in the monkey brain. The blocking of specific binding by the sigma-1 selective ligand FTC-146, albeit low, is intriguing, and may be due to the biological interaction between the sigma-1 and NMDA receptors. However, the low sigma-1 binding affinity of (*R*)-OF-Me-NB1 measured in vitro (K_i >100 nM) suggests that this is unlikely to reflect sigma-1 binding by the radiotracer. This is also supported by PET studies in rodents, where no difference was observed in the time-activity curves of sigma1R knockout mice and the respective wild-type animals [22].

Conclusion

We have successfully synthesized and performed a comprehensive evaluation of (*R*)-[^{18}F]OF-Me-NB1 as a selective radioligand for GluN2B in non-human primates. This novel radiotracer exhibits favorable metabolic, pharmacokinetic and *in vivo* binding profiles. Given the promising *in vivo* characteristics of (*R*)-[^{18}F]OF-Me-NB1 in monkey brain, this radioligand holds promise for translating into humans.

Declarations

ACKNOWLEDGMENT

The authors thank the staff at the Yale PET Center for their expert technical assistance. Financial support for this study was provided by NIH grants U01MH107803 and also partly supported by the Swiss National Science Foundation (Grants numbers 310030E-160403/1 and 310030E-182872/1) to S. M. Ametamey.

COMPLIANCE WITH ETHICAL STANDARDS:

Conflict of Interest: All authors declare that he/she has no conflict of interest.

Ethical approval: PET imaging experiments were performed in rhesus monkeys (Macaca mulatta) according to a protocol approved by the Yale University Institutional Animal Care and Use Committee. All applicable international, national, and institutional guidelines for the care and use of animals were followed.

References

1. Ouyang X, Mukherjee J, Yang ZY. Synthesis, radiosynthesis, and biological evaluation of fluorinated thienylcyclohexyl piperidine derivatives as potential radiotracers for the NMDA receptor-linked calcium ionophore. Nucl Med Biol. 1996;23:315-24. doi:10.1016/0969-8051(95)02086-1.

2. Ametamey SM, Bruehlmeier M, Kneifel S, Kokic M, Honer M, Arigoni M, et al. PET studies of [^{18}F]-memantine in healthy volunteers. Nucl Med Biol. 2002;29:227-31. doi:10.1016/s0969-8051(01)00293-1.

3. Zhou HY, Chen SR, Byun HS, Chen H, Li L, Han HD, et al. N-methyl-D-aspartate receptor- and calpain-mediated proteolytic cleavage of K^+-Cl^- cotransporter-2 impairs spinal chloride homeostasis in neuropathic pain. J Biol Chem. 2012;287:33853-64. doi:10.1074/jbc.M112.395830.

4. Salabert AS, Fonta C, Fontan C, Adel D, Alonso M, Pestourie C, et al. Radiolabeling of [^{18}F]-fluoroethylnormemantine and initial in vivo evaluation of this innovative PET tracer for imaging the PCP sites of NMDA receptors. Nucl Med Biol. 2015;42:643-53. doi:10.1016/j.nucmedbio.2015.04.001.

5. Salabert AS, Mora-Ramirez E, Beaurain M, Alonso M, Fontan C, Tahar HB, et al. Evaluation of [^{18}F]FNM biodistribution and dosimetry based on whole-body PET imaging of rats. Nucl Med Biol. 2018;59:1-8. doi:10.1016/j.nucmedbio.2017.12.003.

6. Orita K, Sasaki S, Maeda M, Hashimoto A, Nishikawa T, Yugami T, et al. Synthesis and evaluation of 1-(1-[5-(2'-[^{18}F]fluoroethyl)-2-thienyl]-cyclohexyl)piperidine as a potential in vivo radioligand for the NMDA receptor-channel complex. Nucl Med Biol. 1993;20:865-73. doi:10.1016/0969-8051(93)90153-l.

7. Bhatt JM, Prakash A, Suryavanshi PS, Dravid SM. Effect of ifenprodil on GluN1/GluN2B N-methyl-D-aspartate receptor gating. Mol Pharmacol. 2013;83:9-21. doi:10.1124/mol.112.080952.

8. Ahmed H, Haider A, Ametamey SM. N-Methyl-D-Aspartate (NMDA) receptor modulators: a patent review (2015-present). Expert Opin Ther Pat. 2020;30:743-67. doi:10.1080/13543776.2020.1811234.

9. Singh R, Ganeshpurkar A, Kumar D, Kumar D, Kumar A, Singh SK. Identifying potential GluN2B subunit containing N-Methyl-D-aspartate receptor inhibitors: an integrative in silico and molecular modeling approach. J Biomol Struct Dyn. 2020;38:2533-45. doi:10.1080/07391102.2019.1635530.

10. Devadasan C, Starr B, Doyle KM. Effect of N1-dansylspermine and Ro25,6981 on locomotor activity in naive mice and in the reserpinized mouse model of Parkinson's disease. Neuroreport. 2016;27:1243-7. doi:10.1097/WNR.0000000000000685.

11. Schreiber JA, Schepmann D, Frehland B, Thum S, Datunashvili M, Budde T, et al. A common mechanism allows selective targeting of GluN2B subunit-containing N-methyl-D-aspartate receptors. Commun Biol. 2019;2:420. doi:10.1038/s42003-019-0645-6.

12. Wang XS, Zhang ZR, Zhang XR, Chen SY, Shao B, Xie CL. Modulation of CaMKIIa-GluN2B interaction in levodopa-induced dyskinesia in 6-OHDA-lesioned Parkinson's rats. Biomed Pharmacother. 2018;107:769-76. doi:10.1016/j.biopha.2018.08.062.

13. Menniti FS, Lindsley CW, Conn PJ, Pandit J, Zagouras P, Volkmann RA. Allosteric modulators for the treatment of schizophrenia: targeting glutamatergic networks. Curr Top Med Chem. 2013;13:26-54. doi:10.2174/1568026611313010005.

14. He Y, Mu L, Ametamey SM, Schibli R. Recent progress in allosteric modulators for GluN2A subunit and development of GluN2A-selective nuclear imaging probes. J Labelled Comp Radiopharm. 2019;62:552-60. doi:10.1002/jlcr.3744.

15. McGinnity CJ, Arstad E, Beck K, Brooks DJ, Coles JP, Duncan JS, et al. Comment on " In Vivo [^{18}F]GE-179 Brain Signal Does Not Show NMDA-Specific Modulation with Drug Challenges in Rodents and Nonhuman Primates". ACS Chem Neurosci. 2019;10:768-72. doi:10.1021/acschemneuro.8b00246.

16. Sobrio F, Gilbert G, Perrio C, Barre L, Debruyne D. PET and SPECT imaging of the NMDA receptor system: an overview of radiotracer development. Mini Rev Med Chem. 2010;10:870-86. doi:10.2174/138955710791608299.

17. Schepmann D, Frehland B, Lehmkuhl K, Tewes B, Wunsch B. Development of a selective competitive receptor binding assay for the determination of the affinity to NR2B containing NMDA receptors. J Pharm Biomed Anal. 2010;53:603-8. doi:10.1016/j.jpba.2010.04.014.

18. Perin-Dureau F, Rachline J, Neyton J, Paoletti P. Mapping the binding site of the neuroprotectant ifenprodil on NMDA receptors. J Neurosci. 2002;22:5955-65. doi:20026631.

19. Tewes B, Frehland B, Schepmann D, Schmidtke KU, Winckler T, Wunsch B. Conformationally constrained NR2B selective NMDA receptor antagonists derived from ifenprodil: Synthesis and biological evaluation of tetrahydro-3-benzazepine-1,7-diols. Bioorg Med Chem. 2010;18:8005-15. doi:10.1016/j.bmc.2010.09.026.

20. Kramer SD, Betzel T, Mu L, Haider A, Herde AM, Boninsegni AK, et al. Evaluation of [^{11}C]Me-NB1 as a Potential PET Radioligand for Measuring GluN2B-Containing NMDA Receptors, Drug Occupancy, and Receptor Cross Talk. J Nucl Med. 2018;59:698-703. doi:10.2967/jnumed.117.200451.

21. Rischka L, Vraka C, Pichler V, Rasul S, Nics L, Gryglewski G, et al. First-in-human brain PET imaging of the GluN2B-containing N-methyl-D-aspartate receptor with (*R*)-[^{11}C]Me-NB1. J Nucl Med. 2021. doi:10.2967/jnumed.121.262427.

22. Haider A, Iten I, Ahmed H, Muller Herder A, Gruber S, Kramer SD, et al. Identification and Preclinical Evaluation of a Radiofluorinated Benzazepine Derivative for Imaging the GluN2B Subunit of the Ionotropic NMDA Receptor. J Nucl Med. 2018. doi:10.2967/jnumed.118.212134.

23. Haider A, Herde AM, Kramer SD, Varisco J, Keller C, Frauenknecht K, et al. Preclinical Evaluation of Benzazepine-Based PET Radioligands (*R*)- and (*S*)-[^{11}C]Me-NB1 Reveals Distinct Enantiomeric Binding Patterns and a Tightrope Walk Between GluN2B- and sigma1-Receptor-Targeted PET Imaging. J Nucl Med. 2019;60:1167-73. doi:10.2967/jnumed.118.221051.

24. Li S, Cai Z, Zheng MQ, Holden D, Naganawa M, Lin SF, et al. Novel [^{18}F]-Labeled kappa-Opioid Receptor Antagonist as PET Radiotracer: Synthesis and In Vivo Evaluation of [^{18}F]LY2459989 in Nonhuman Primates. J Nucl Med. 2018;59:140-6. doi:10.2967/jnumed.117.195586.

25. Li S, Zheng MQ, Naganawa M, Kim S, Gao H, Kapinos M, et al. Development and In Vivo Evaluation of a kappa-Opioid Receptor Agonist as a PET Radiotracer with Superior Imaging Characteristics. J Nucl Med. 2019;60:1023-30. doi:10.2967/jnumed.118.220517.

26. Zheng MQ, Nabulsi N, Kim SJ, Tomasi G, Lin SF, Mitch C, et al. Synthesis and evaluation of [^{11}C]-LY2795050 as a kappa-opioid receptor antagonist radiotracer for PET imaging. J Nucl Med. 2013;54:455-63. doi:10.2967/jnumed.112.109512.

27. Ichise M, Toyama H, Innis RB, Carson RE. Strategies to improve neuroreceptor parameter estimation by linear regression analysis. J Cereb Blood Flow Metab. 2002;22:1271-81. doi:10.1097/01.WCB.0000038000.34930.4E.

28. Cunningham VJ, Rabiner EA, Slifstein M, Laruelle M, Gunn RN. Measuring drug occupancy in the absence of a reference region: the Lassen plot re-visited. J Cereb Blood Flow Metab. 2010;30:46-50. doi:10.1038/jcbfm.2009.190.

29. Kohl BK, Dannhardt G. The NMDA receptor complex: a promising target for novel antiepileptic strategies. Curr Med Chem. 2001;8:1275-89. doi:10.2174/0929867013372328.

30. James ML, Shen B, Zavaleta CL, Nielsen CH, Mesangeau C, Vuppala PK, et al. New positron emission tomography (PET) radioligand for imaging sigma-1 receptors in living subjects. J Med Chem. 2012;55:8272-82. doi:10.1021/jm300371c.

Figures

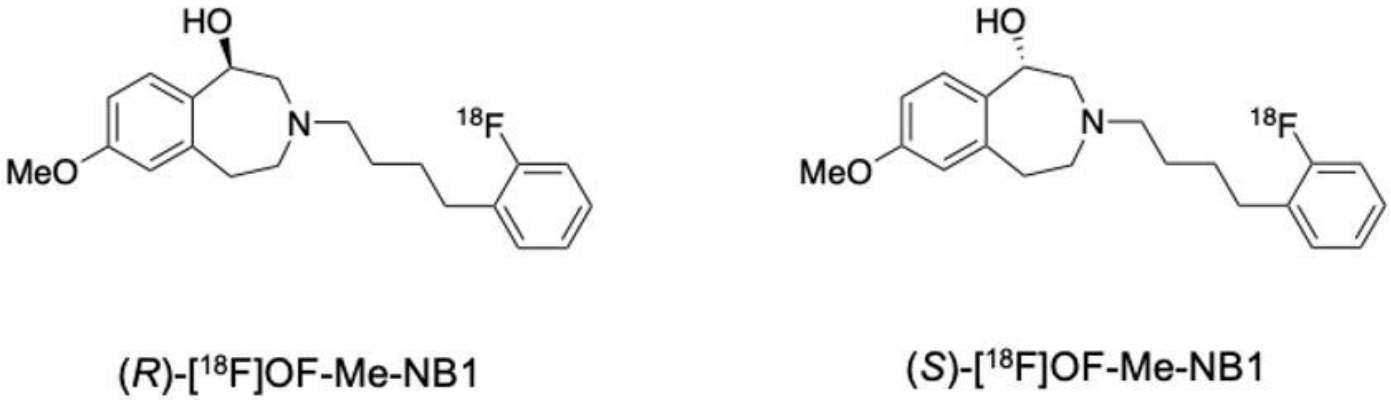

Figure 1

Chemical structures of (R) and (S)-[18F]OF-Me-NB1.

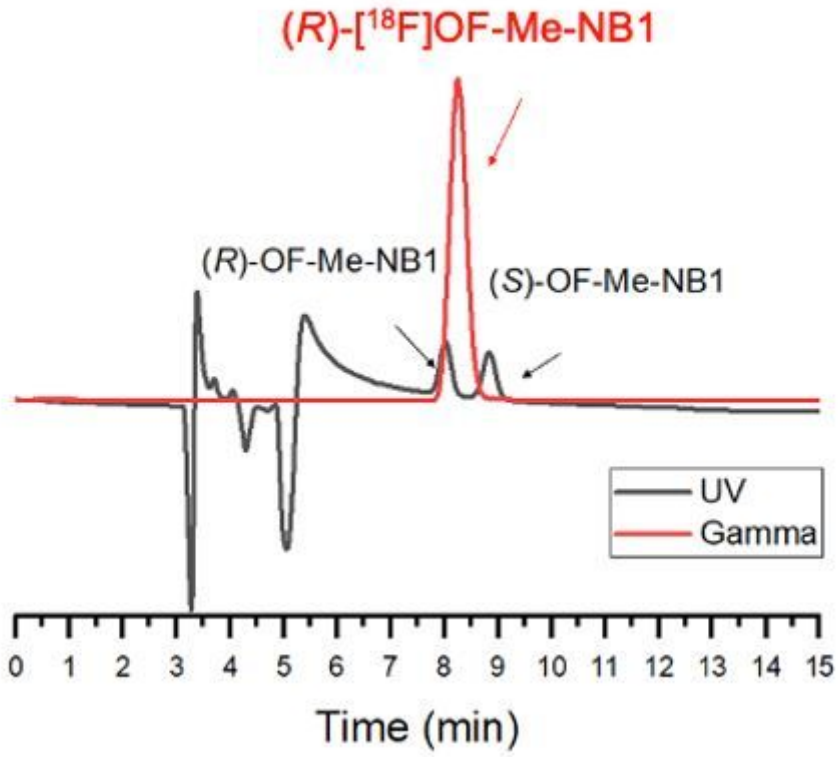

Figure 2

A representative analytical chiral HPLC chromatogram for (R)-[18F]-OF-Me-NB1(red, gamma), co-injected with the racemic reference standard (black, UV). Column: Daicel chiral Pak@IA, 250 x 4.6 mm, 5 µm. Mobile phase: 90/10 hexane/EOH. Flow rate: 1 mL/min.

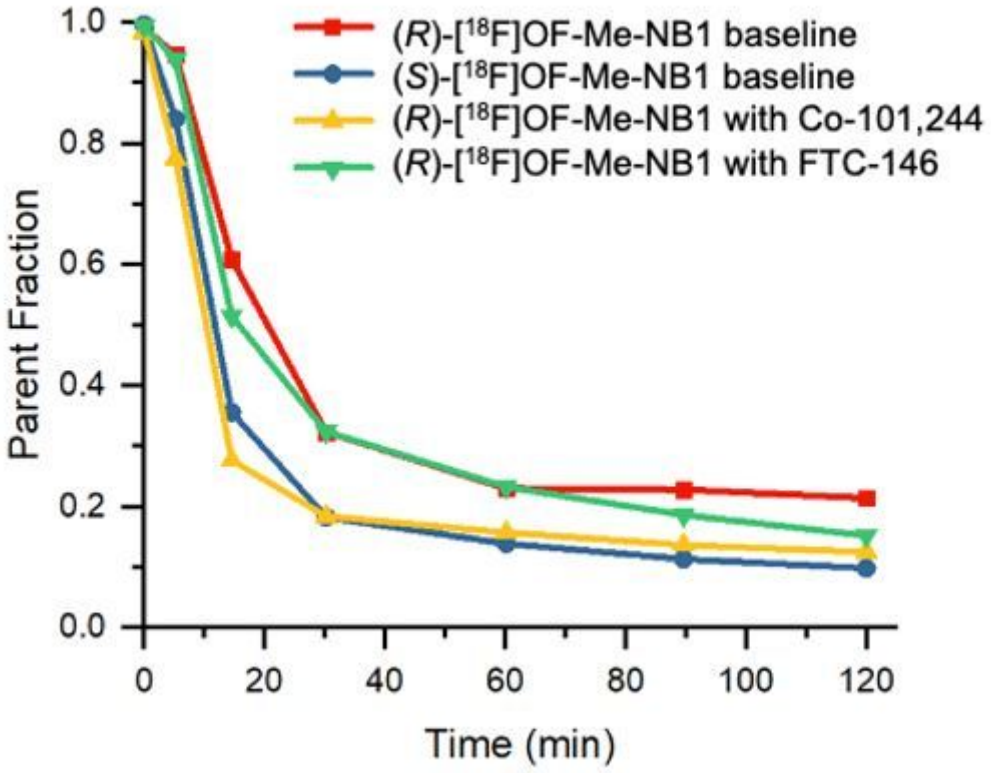

Figure 3

Parent fraction of (R)- and (S)-[18F]OF-Me-NB1 over time in the same monkey.

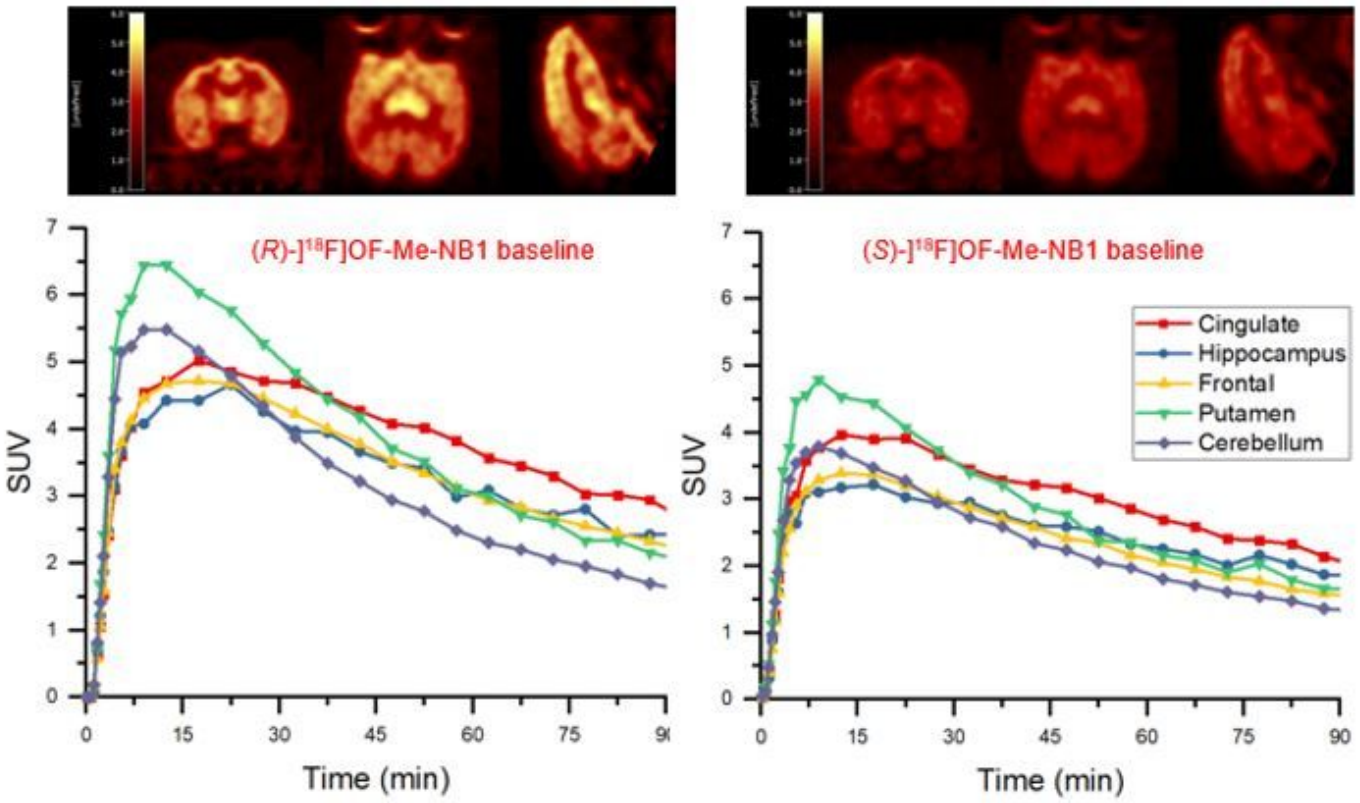

Figure 4

PET images of (R)- and (S)-[18F]OF-Me-NB1, summed from 30 to 45 min, in the same monkey brain (top), and the corresponding time-activity curves (bottom).

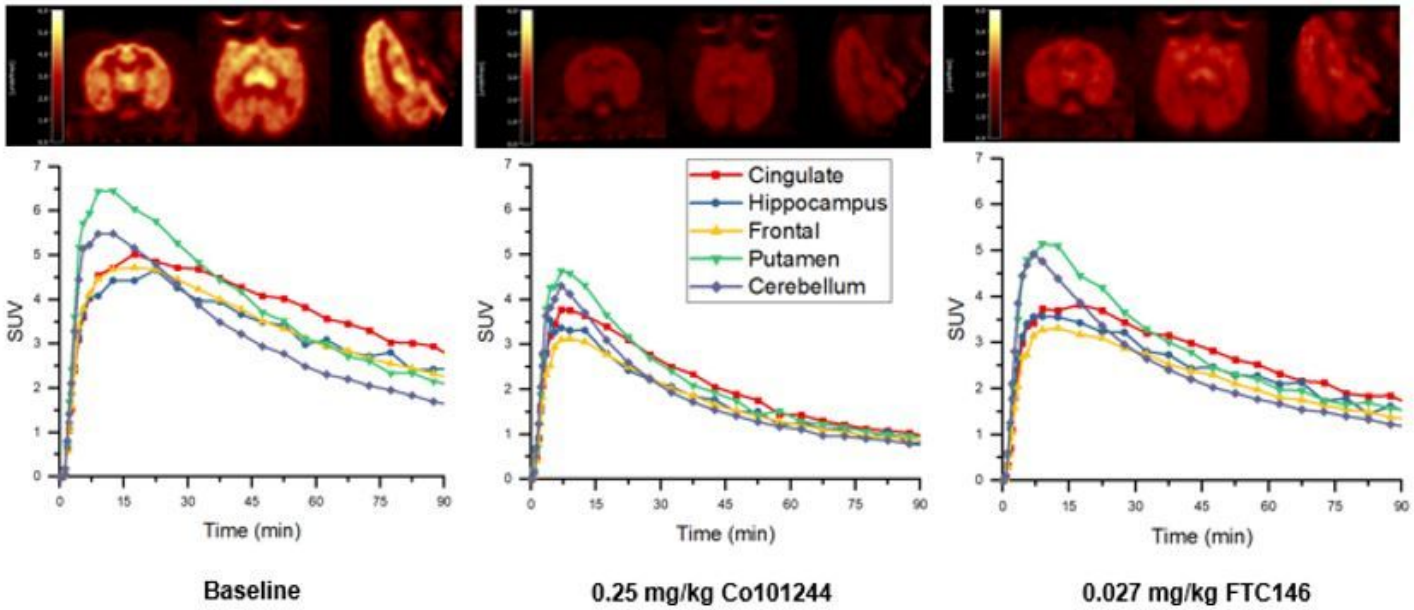

Figure 5

PET images of (R)-[18F]OF-Me-NB1 summed from 30 to 45 min, for the baseline scan (top left), and blocking scans with Co101,244 (0.25 mg/kg, top middle) and FTC-146 (0.027 mg/kg, top right), and the corresponding time activity curves (bottom).

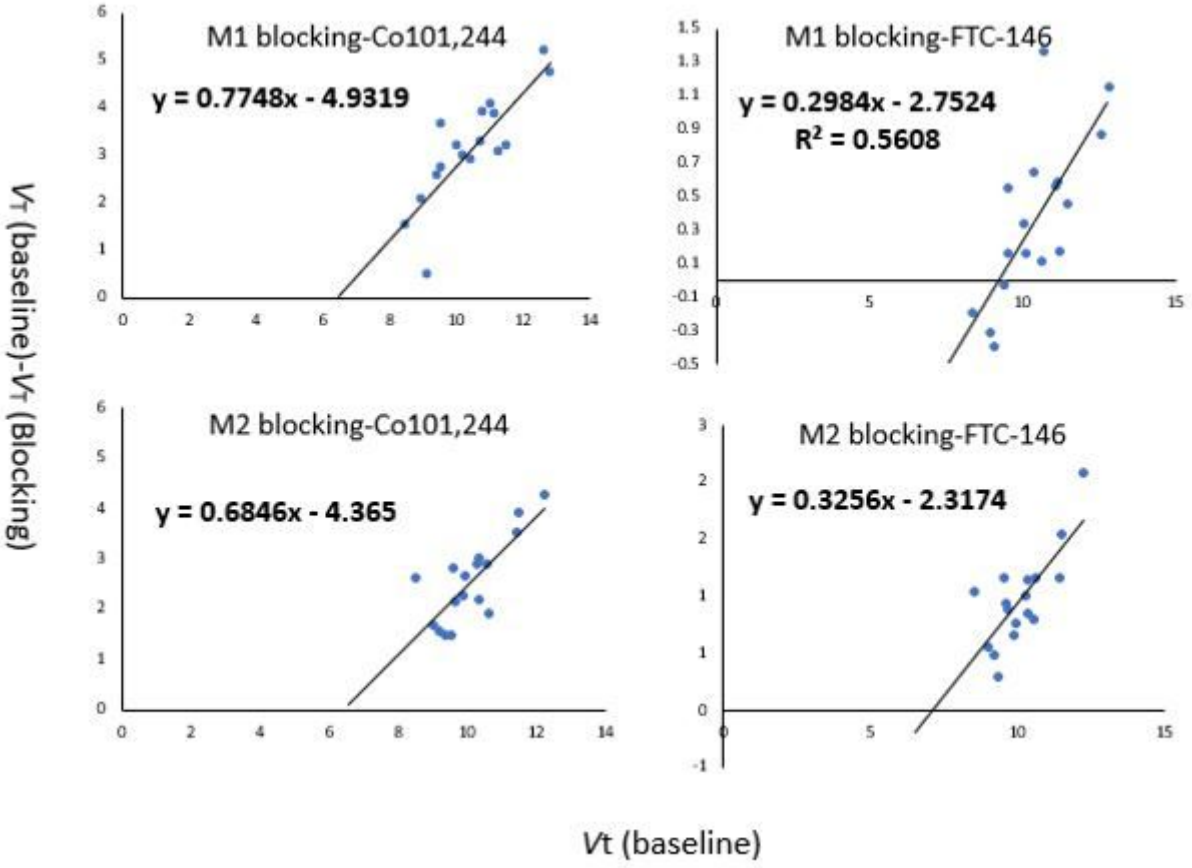

Figure 6

Receptor occupancy plots for (R)-[18F]OF-Me-NB1 blocking scans with Co101,244 (0.25 mg/kg) or FTC-146 (0.027 and 0.125 mg/kg, respectively) in two different monkeys (M1 and M2).